JOURNAL OF APPLIED ELECTROCHEMISTRY 25 (1995) 433–440

Degradation mechanisms of nickel oxide electrodes in zinc/nickel oxide cells with low-zinc-solubility electrolytes

R. F. PLIVELICH, F. R. McLARNON, E. J. CAIRNS

Energy & Environment Division, Lawrence Berkeley Laboratory and Department of Chemical Engineering, University of California, Berkeley, CA 94720, USA

Received 20 May 1994; revised 28 September 1994

Nickel oxide electrodes that suffered capacity degradation during extended cycling in zinc/nickel oxide cells were examined by a variety of chemical and physical techniques. Nickel hydroxyzincates, which have been speculated to cause such capacity degradation, were also examined. Powder X-ray diffraction experiments indicated that the intersheet distance between layers of turbostratic nickel hydroxide increased when zinc was incorporated. Photoelectron spectra (XPS) showed that this material is probably a mixture of $Ni(OH)_2$ and ZnO or $Zn(OH)_2$. Raman spectroscopy data also supported this conclusion. XPS indicated that the form of zinc in degraded nickel oxide electrodes is probably ZnO or $Zn(OH)_2$. Significant increases in resistivity were found in cycled nickel oxide electrodes, and optical microscopy provided visible evidence of mechanical damage during cycling. These results suggest that the observed capacity degradation was largely mechanical in nature, and not due to the formation of nickel–zinc double hydroxides, as had been reported by others. Cell-cycling experiments indicated that the mechanical degradation is largely irreversible.

1. Introduction

The zinc/nickel oxide (Zn/NiOOH) cell, with its features of good specific energy, excellent specific power, and use of relatively nontoxic component materials, is a potentially attractive system for use in powering portable electronic devices and electric vehicles. Recent advances [1] have extended the durability of this system to more than 500 cycles in 1.4 Ah laboratory test cells. This cycle life extension was achieved through the use of sealed cell technology, and electrolytes containing lower concentrations of KOH than that traditionally employed (a typical combination is 4.5 M KOH, 1.8 M K_2CO_3 and 1.8 M KF against the 6 M KOH and 1 M LiOH previously used). This electrolyte formulation mitigates two primary problems of the negative electrode of the Zn/NiOOH cell: dendritic shorting and shape change. It was reported in [1] that the capacity of a Zn/NiOOH cell with KOH–K_2CO_3–KF electrolyte was limited by the nickel oxide electrode (as demonstrated by individual electrode overpotential measurements) throughout the cell lifetime. To achieve greater cycle life, it has become apparent that the durability of the nickel oxide electrode in the zinc/nickel oxide system must be further improved. The degradation of nickel oxide electrode capacity observed in long-lived Zn/NiOOH cells with KOH–K_2CO_3–KF electrolyte is not apparent in Zn/NiOOH cells cycled with the usual concentration of electrolyte, because the latter cells can become capacity-limited by zinc electrode problems and do not cycle for a sufficiently long time for degradation of the nickel oxide electrode to become apparent.

Several causes of capacity loss in nickel oxide electrodes have been postulated. Perhaps the most common, and the least well-quantified process, is the loss of wetting of the electrode pores during cycling. When the end of cell charge of a nickel oxide electrode is approached, an oxygen evolution reaction begins to compete with the nickel oxidation reaction [2]. This reaction can force electrolyte from electrode pores, thereby drying the electrode and causing a loss of capacity. The oxygen evolution reaction on metallic nickel, nickel oxides and hydroxides, and other materials has been studied by many investigators [2–6], and will not be considered further in this work.

Another mode of capacity loss is thought to be mechanical damage of the sintered nickel current collector during cycling, with accompanying isolation of nickel active material from the current-collecting structure. In the early 1980s Fritts addressed this issue [7]. In one study, by manipulating the preparation conditions of a nickel oxide electrode, he found that he could induce the formation of blisters within the electrode during cycling. It was concluded that the blistering was caused by the formation of macropores in the electrode, which served as collection points for oxygen evolved during cell charging. These macropores, in turn, were thought to be caused by a gradient in the rigidity of the sintered nickel substrate in the direction away from the current-collecting grid. No blistering was

0021-891X

observed when oxygen evolution was avoided. In a later study [8], Fritts found that the resistivity increase of a sintered nickel oxide electrode generally followed the capacity loss of the electrode. He then concluded that this resistivity increase reflected the formation of electrically isolated islands within the electrode. Note that Fritts examined the Cd/NiOOH system, and not the Zn/NiOOH system studied in the present work. A later modelling study by Lanzi and Landau [9] qualitatively supported the conclusions of Fritts.

Another postulated capacity-loss mechanism is the formation of low-conductivity layers during discharge of the electrode. It is known that the conductivity of NiOOH is approximately three orders of magnitude greater than that of $Ni(OH)_2$ [10]. The formation of a layer of relatively non-conductive $Ni(OH)_2$ near the conductive metallic substrate can presumably lead to capacity loss by forcing a large fraction of the current to travel through the nonconductive layer [9, 11]. This degradation mode is related to the sinter-fracture mode, in the sense that current is being forced to travel through paths of high resistivity.

A mode of failure specifically associated with Zn/NiOOH cells is the precipitation of ZnO or $Zn(OH)_2$ in the pores of the nickel oxide electrode [12]. This process reduces the active area accessible to the electrolyte, thereby decreasing the electrode capacity. In one case, it was found possible to recover the capacity of failing nickel oxide electrodes in a Zn/NiOOH cell by washing in hot 10 N KOH, although published details were sparse [13]. Formation of 'nickel hydroxyzincates' [14] has also been suspected of causing nickel oxide electrode capacity loss in Zn/NiOOH cells [15, 16].

An argument against either ZnO precipitation or the formation of electrochemically inactive zinc-nickel oxide compounds being important capacity-loss mechanisms is the observation that almost all mobile zinc transfers to the nickel oxide electrode within the first few cycles, whereas cell capacity loss occurs more gradually [1, 17], over tens or hundreds of cycles. Because the zinc electrode is typically taken as the life-limiting electrode of Zn/NiOOH cells, there has been few investigations of the degradation modes of nickel oxide electrodes in such cells.

2. Experimental procedures

Several standard materials were synthesized in order to provide a basis for comparison with cycled nickel oxide electrode materials. The method of Faure *et al.* [18] was used to produce α-$Ni(OH)_2$. It involves using concentrated NH_4OH solution (Mallinckrodt, AR grade) to precipitate the hydroxide from an aqueous $Ni(NO_3)_2$ solution (J. T. Baker, 'Baker Analyzed' grade). Several nickel hydroxyzincates, in stoichiometric Ni : Zn ratios of 10 : 1 and 1 : 1, were prepared according to a method published by Romanov [15]. This method is analogous to that of Faure *et al.* [18] for the synthesis of α-$Ni(OH)_2$, except that a starting solution of $Ni(NO_3)_2$ and $Zn(NO_3)_2$ was used. Other standard materials were obtained from commercial sources and included β-$Ni(OH)_2$ ('battery grade', Inco, Ltd), ZnO (Aldrich, 99.999%), and $Zn(OH)_2$ (Alfa).

Powder X-ray diffraction (Siemens unit, copper anode) was found useful for the determination of long-range order and preliminary material characterization. Additional information concerning the lattice structure of nickel hydroxyzincates was obtained using Raman spectroscopy. The region from 280 to 510 cm^{-1} was scanned to observe lattice vibrational modes, if present. The excitation source was a Coherent 90-5 argon-ion laser (514.5 nm, 50 mW focused on sample.) The Raman-scattered light was directed to a Spex 1403 double monochromator and detected with a thermoelectric-cooled RCA 31034 photomultiplier tube. The apparatus was controlled with a Spex Datamate data acquisition system.

Of primary interest is the determination of species which exist on the surface of cycled nickel oxide electrodes. X-ray photoelectron spectroscopy (XPS) was employed for this purpose because of its high surface sensitivity and its ability to distinguish between chemical states. A Perkin–Elmer PHI 5300 unit was used, with a Mg X-ray source (500 W, 15 kV). Charging effects were accounted for by referencing to the adventitious carbon 1*s* peak. In all cases, the pressure inside the UHV chamber was 5.3×10^{-6} N m^{-2} or lower.

As mentioned above, Fritts [7, 8] observed a general resistivity increase of nickel oxide electrodes during extended cycling in Cd/NiOOH cells, however his studies measured only the average resistivity increase within an entire electrode. It is useful to determine if a resistivity increase occurs in electrodes cycled in a reduced-alkalinity electrode. In addition, it is appropriate and instructive to measure the spatial dependence of any observed resistivity increase.

Samples were harvested from a 21 Ah Zn/NiOOH cell pack which consisted of three pasted zinc electrodes interleaved between four nickel oxide electrodes; electrode dimensions were 15 cm × 16 cm. All nickel oxide electrodes used porous sintered nickel current collectors and were purchased from Eagle–Picher Industries, Inc. The loading of active material in the nickel oxide electrodes was 1.6 g cm^{-3} void space, which is somewhat higher than the 1.3 g cm^{-3} void space loading that has been most common for other nickel electrodes studied in this laboratory [1]. The cell pack was assembled with nickel oxide electrodes of two different thicknesses: 0.94 mm (37 mils) and 0.46 mm (18 mils). Each of the thicker full-capacity nickel oxide electrodes was surrounded by two zinc electrodes, and the thinner half-capacity nickel oxide electrodes were placed at the ends of the cell pack. This construction technique assured that each electrode was charged and discharged at the same rate, and provided a reasonable simulation of a much larger pack. The total zinc electrode

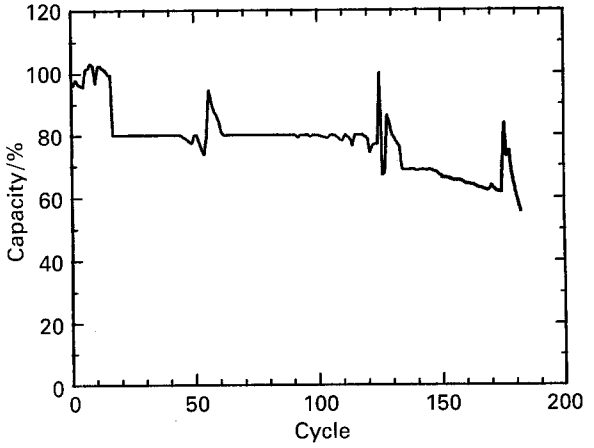

Fig. 1. Cycling behaviour of a 21 Ah Zn/NiOOH cell utilizing a reduced alkalinity electrolye [19]. The cell capacity is expressed as a fraction of the full NiOOH electrode capacity established early in cell life. Cycles: (1–20) DOD = 100%; (21–125) DOD = 80% and (126–185) DOD = 100%.

capacity was three times that of the total nickel oxide electrode capacity, and the zinc electrodes consisted of 94 wt% ZnO, 4 wt% PTFE, and 2 wt% PbO. The cell contained a reduced-alkalinity electrolyte (3.2 M KOH, 1.8 M KF, 1.8 M K_2CO_3, ZnO saturated) and failed after 200 cycles due to gradual capacity loss.

Figure 1 displays the capacity against cycle number behaviour of this cell [19]. The cell was charged at a $C/7$ rate until a cell voltage of 1.95 V was reached, after which the cell voltage was held at 1.95 V until ~105% of the previous cycle discharge capacity was recharged. The typical discharge was at a $C/3$ rate to a cell voltage of 1.0 or 80% depth of discharge (DOD), whichever condition arose first. The apparent capacity excursions at cycles 55, 125 and 175 represent 'regeneration' cycles, which consisted of a $C/10$ discharge to a cell voltage of 0 V followed by a $C/10$ charge, and were intended to help recover some of the lost capacity of the cell. For further details of cell fabrication and operation, consult Adler *et al.* [1].

The resistance measurements were of the four-point probe type, to reduce any errors due to contact resistance. The current source was a PAR 273 potentiostat/galvanostat, operating in galvanostatic mode. Cycled nickel oxide electrodes were sectioned into samples measuring 4 cm × 0.35 cm. A low-speed wafering saw with a high concentration diamond blade (Buehler) was used to minimize damage to the electrode material.

The post-cycling galvanostatic charge/discharge experiments were of the standard three-electrode type. The working electrode was of the same cycled electrode material as was used in the resistivity measurements. The counter electrode was constructed of initially uncycled nickel oxide material, subjected to five formation cycles in an electrolyte of 5.9 M KOH (diluted from 45 w/o KOH, J. T. Baker, 'Baker Analyzed' grade) and 1.1 M LiOH (EM Science, reagent grade). All water used was obtained from a Millipore high resistivity water purification system ($\rho = 15\,M\Omega\,cm$ or greater). The superficial dimensions of both electrodes were 9.5 mm × 10.5 mm, and a Hg/HgO reference electrode was used. Pellon 2524 nonwoven nylon wicking material (Freudenberg Nonwoven, Chelmsford, Massachusetts) provided wetting and mechanical separation of the electrodes. The electrolyte used in all post-cycling experiments was 5.9 M KOH and 1.1 M LiOH, with an excess of ZnO (EM Science, reagent grade) added to achieve saturation. In most instances, a small amount (0.37 or 1.1 g dm^{-3}) of surfactant Triton X-100 was added. The electrode was charged at a $C/6$ rate (53 A m^{-2}), followed by a potentiostatic taper charge at a potential of 530 mV vs Hg/HgO, for a total charging time of ~ 6 h, and a 15 min open-circuit period. The cell was then discharged at a $C/6$ rate until the working electrode reached a potential of 0 mV vs Hg/HgO. In some cases, the cell was charged and discharged more slowly ($C/15$ rate = 21 A m^{-2}) to obtain information on the rate dependence of the capacity.

The goals of these experiments were to provide key comparative measurements. Initially, several cycles of the electrode were carried out in a surfactant-free electrolyte to establish a relatively stable baseline capacity. Then, various modifying treatments were applied in series. To test the idea that a loss of wetting may cause a capacity loss in nickel oxide electrodes, the electrodes were operated in an electrolyte containing Triton X-100 (Spectrum Chemical, Gardenas, CA). No attempt was made to find either an optimal wetting agent for the system, or an optimal concentration of surfactant. The intent was only to determine if a commonly available wetting agent would influence the measured discharge capacity of the electrode. After this treatment, the nickel oxide electrode was washed twice in 20 w/o KOH to remove any zinc species which could presumably contribute to a capacity loss. The first washing was at 20 °C for 18 h, and fresh KOH was used for the second washing at 60 °C for 18 h. Finally, the electrodes were cycled under various degrees of mechanical compression, to determine if it was possible to reverse the (presumed) loss of contact between active material and current collector.

3. Results and discussion

As already noted, there has been speculation that a nickel hydroxyzincate species may be responsible for some capacity loss in nickel oxide electrodes used in Zn/NiOOH cells. Two nickel hydroxyzincates were prepared, one with a Ni : Zn ratio of 1 : 1 and the other with a Ni : Zn ratio of 10 : 1. Figure 2 compares the powder X-ray diffraction patterns of α-$Ni(OH)_2$ and the nickel hydroxyzincates. As stated by Bode [14] and Romanov [15], the α-$(Ni,Zn)(OH)_2$ materials have the same general long-range order as α-$Ni(OH)_2$; i.e., a brucite structure. Changes in the (0 0 1) d-spacing imply that the intersheet distance

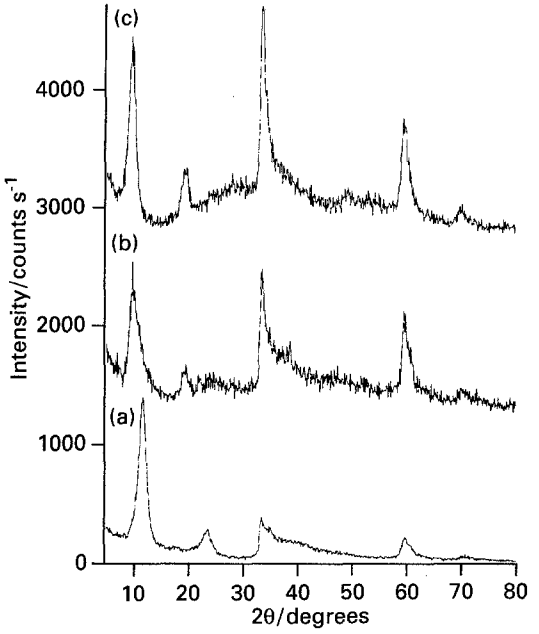

Fig. 2. Powder X-ray diffraction patterns for (a) α-$Ni(OH)_2$ and nickel hydroxyzincates with Ni : Zn ratios of (b) 1 : 1 and (c) 10 : 1.

becomes greater when zinc is included in the $Ni(OH)_2$ material.

The Zn $2p_{3/2}$ photoelectron spectra of α-(Ni,Zn)-$(OH)_2$ (Ni : Zn = 10 : 1) and $Zn(OH)_2$ are compared in Fig. 3, which shows good agreement in their binding energies. Also, the binding energy of the α-$(Ni,Zn)(OH)_2$ (Ni : Zn = 1 : 1) was found to be in agreement with that for ZnO.

In an attempt to clarify the ambiguity concerning the nature of the nickel hydroxyzincates, Raman spectroscopy was used. Figure 4 displays the Raman spectra of α-$Ni(OH)_2$ and 1 : 1 α-$(Ni,Zn)(OH)_2$. The region scanned is characteristic of lattice vibrational modes of both nickel and zinc hydroxides. Presumably, if zinc is substituted for nickel to form a 'true' nickel

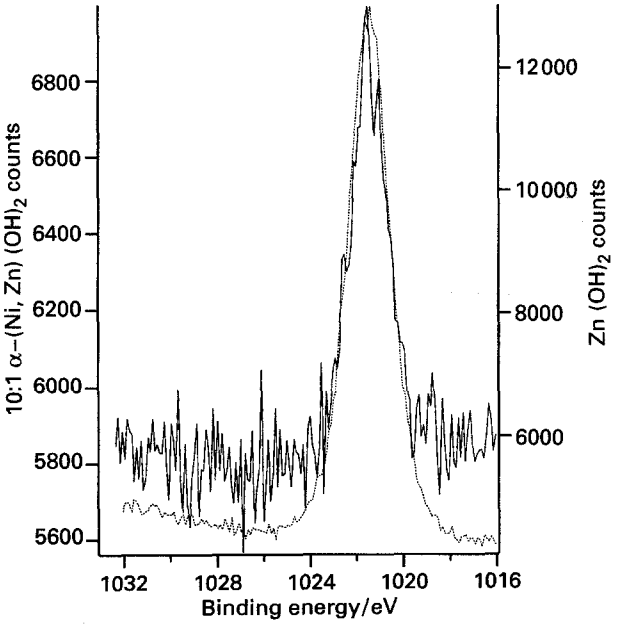

Fig. 3. Zn $2p_{3/2}$ photoelectron spectra of α-$(Ni,Zn)(OH)_2$ (Ni : Zn = 10 : 1) and $Zn(OH)_2$. Curves: (——) 10 : 1 α-(Ni,Zn)-$(OH)_2$ and (·····) $Zn(OH)_2$.

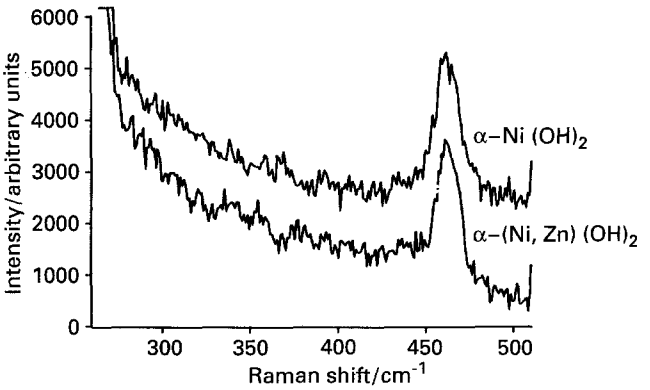

Fig. 4. Raman spectra of α-$Ni(OH)_2$ and 1 : 1 $\alpha(Ni,Zn)(OH)_2$.

hydroxyzincate compound, the Ni–O lattice mode would be altered to some extent. As the figure shows, only the Ni–O vibrational mode is present [e.g. 20], with both the peak position and full-width at half-maximum (FWHM) being the same in both spectra. No band characteristic of a Zn–O vibrational mode is present, although some forms of $Zn(OH)_2$ are known to lack Raman activity in this region [21]. In summary, Raman spectroscopy suggests that the nickel hydroxyzincate is probably a coprecipitate of α-$Ni(OH)_2$ and a form of $Zn(OH)_2$ lacking the structural order to render it Raman active.

Further work needs to be done in characterizing these nickel hydroxyzincates. Bode *et al.* [14] state that these compounds exhibit X-ray diffraction patterns similar to that of α-$Ni(OH)_2$, as was confirmed here. Because none of these compounds exhibits long-range order, a better method of structural characterization, such as EXAFS, should be utilized.

An important question to be addressed by the present work is whether the use of a reduced-alkalinity electrolyte in a Zn/NiOOH cell will induce observable chemical or structural changes in the nickel oxide electrode, such as the formation of nickel hydroxyzincates, or of water-insoluble fluoride or carbonate species. These species could presumably block the electroactive surface of the electrode, resulting in capacity loss. The Ni $2p_{3/2}$ spectra of electrode materials cycled in a standard electrolyte and in the reduced-alkalinity electrolyte are compared in Fig. 5. Little binding energy difference is observed between these materials and β-$Ni(OH)_2$. Additional work indicates that the form of zinc present in material cycled in both standard and reduced-alkalinity electrolytes is probably $Zn(OH)_2$ and/or ZnO. There was no fluoride detected by XPS in any of the cycled electrode samples which used a fluoride-containing electrolyte. This result decreases the probability of a nickel fluoride or zinc fluoride compound blocking the pores of the nickel oxide electrode. It appears that by using XPS, one cannot observe a significant difference between nickel oxide electrode materials cycled in standard electrolyte and materials cycled in a reduced-alkalinity electrolyte.

There are several points to be made concerning the

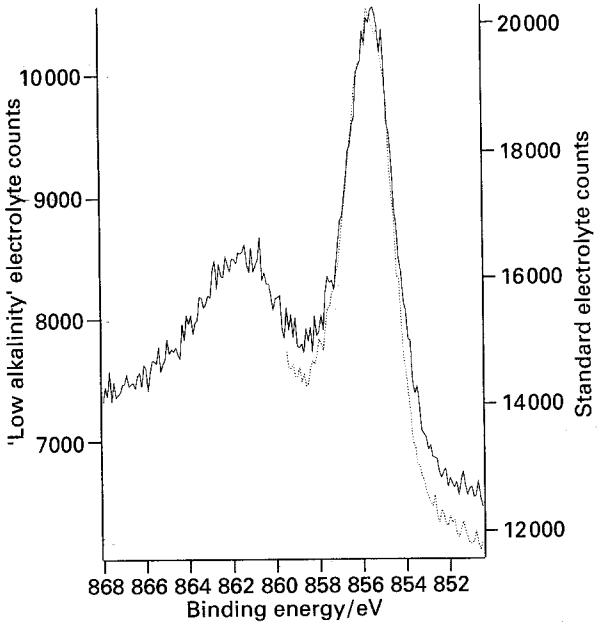

Fig. 5. Ni $2p_{3/2}$ spectra of nickel electrode material cycled in reduced alkalinity electrolyte and in standard electrolyte. Curves: (——) 'low alkalinity' and (·····) standard.

interpretation of these results. In this work, it was decided to rely more upon comparing measured spectra to those of standard materials instead of relying on absolute binding energies, for several reasons. First, there is the question of background signal removal. In the Ni $2p_{3/2}$ region, the background is highly nonlinear. There are many algorithms available to subtract the background, and deconvolute the data, but the issue is by no means settled and is the subject of continuing research. In the literature, the XPS Ni $2p_{3/2}$ spectra of β-$Ni(OH)_2$, which have been reported by several workers [22–27], exhibit a scatter of up to 1.3 eV. In some cases, the method of background subtraction and/or deconvolution was not reported. In others, the methods of preparation and characterization of the nickel hydroxides and nickel oxyhydroxides were not reported. Thus, the safest and simplest method of characterization was the visual comparison of the spectra of standard materials prepared by known synthetic routes with those of the unknown materials.

A second issue is the method of charge correction. The use of adventitious carbon as a method of charge referencing is not accepted by some investigators [28], but others have shown it to be a reproducible method [29]. The use of the so-called Auger parameter, α, is recommended by some as a reliable method of charge correction [28]. The Auger parameter is essentially the difference in apparent binding energies of an Auger peak and a photoelectron peak. By taking the difference between two peaks, charging effects (if constant throughout the entire binding energy range) will cancel. An Auger peak is used in the Auger parameter because in some situations, a greater shift in Auger peaks will be observed than in photoelectron peaks, making it easier to resolve two unknowns. This approach was not used here, because the Auger peaks tended to be quite broad (FWHM of about 5 eV), and nonGaussian in shape. In this case, reliable estimates of the Auger peak position and the Auger parameter are difficult to obtain.

Another concern is the stability of these hydrated nickel and zinc oxides under ultrahigh vacuum. The various nickel oxides of interest differ substantially in their degrees of hydration, which affects their crystal structure, and possibly their response under XPS. One investigator studied water absorption and desorption from nickel hydroxide and nickel oxyhydroxide [30], and found them to be relatively stable with regard to their XPS spectra at room temperature, however this possible uncertainty must be recognized.

The results of the resistivity measurements on cycled nickel oxide electrodes are given in Fig. 6. This figure presents spatial variations in resistivity at a selected region of each nickel oxide electrode, the lower left corner. The resistivity of uncycled 0.46 mm thick sintered nickel oxide electrodes of the type examined here was found to be $7 \times 10^{-5}\,\Omega$ cm, and that of the 0.94 mm thick electrodes was $18 \times 10^{-5}\,\Omega$ cm. There appears to be some variation of resistivity with position for each electrode in the cell pack. This result is interesting, in that other results [7, 8] documenting resistivity increases in cycled nickel electrodes were referring to bulk resistivity of an entire electrode, and not a resistivity 'profile'. Note that the resistivity increase appears to be more pronounced (on a relative basis) in the thicker 0.94 mm electrodes. This trend of greater resistivity increase with increasing electrode thickness has been predicted by numerical modelling [9] and has

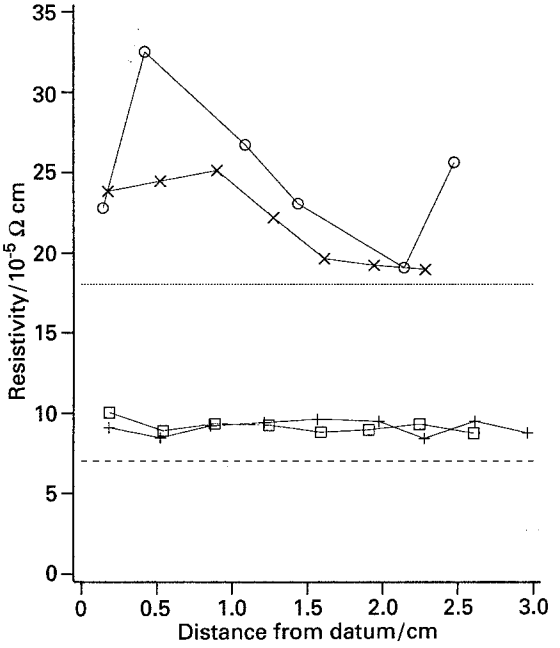

Fig. 6. Conductivity variation of nickel oxide electrodes in the cell pack. The abscissa represents the horizontal distance along each of the four nickel oxide electrodes, measured from the lower corner of the electrode directly below the tab. 'Ni A' and 'Ni D' are half-capacity 0.46 mm thick nickel oxide electrodes located at the two ends of the cell pack and 'Ni B' and 'Ni C' are full-capacity 0.94 mm thick nickel oxide electrodes located in the central region of the cell pack, interleaved between three zinc electrodes. Key: (+) Ni A, (×) Ni B, (○) Ni C, (□) Ni D and (– – –) uncycled 0.46 mm, (·····) uncycled 0.94 mm.

been observed previously [8]. There was evidence of blistering in electrode Ni C, which may account for the large magnitude and erratic nature of the observed resistivity changes.

Optical microscopy was used to examine large-scale structural changes in the electrodes. In general, there was visible evidence of delamination in electrode materials that exhibited the greatest resistivity increase. Figure 7(a) is a cross-sectional view of uncycled nickel oxide electrode material. Figure 7(b) displays the cross section of material that has been cycled to failure. This material was taken from electrode Ni C and prepared as described in the section on resistivity measurements. The magnification in the photographs is about 400×; the thickness of the electrodes is 0.94 mm. Note the relatively large fissures beginning near the wires of the nickel mesh, and extending in a planar fashion throughout the electrode. Among others, Fritts observed this behaviour, and speculated that it may be the precursor to blistering [8].

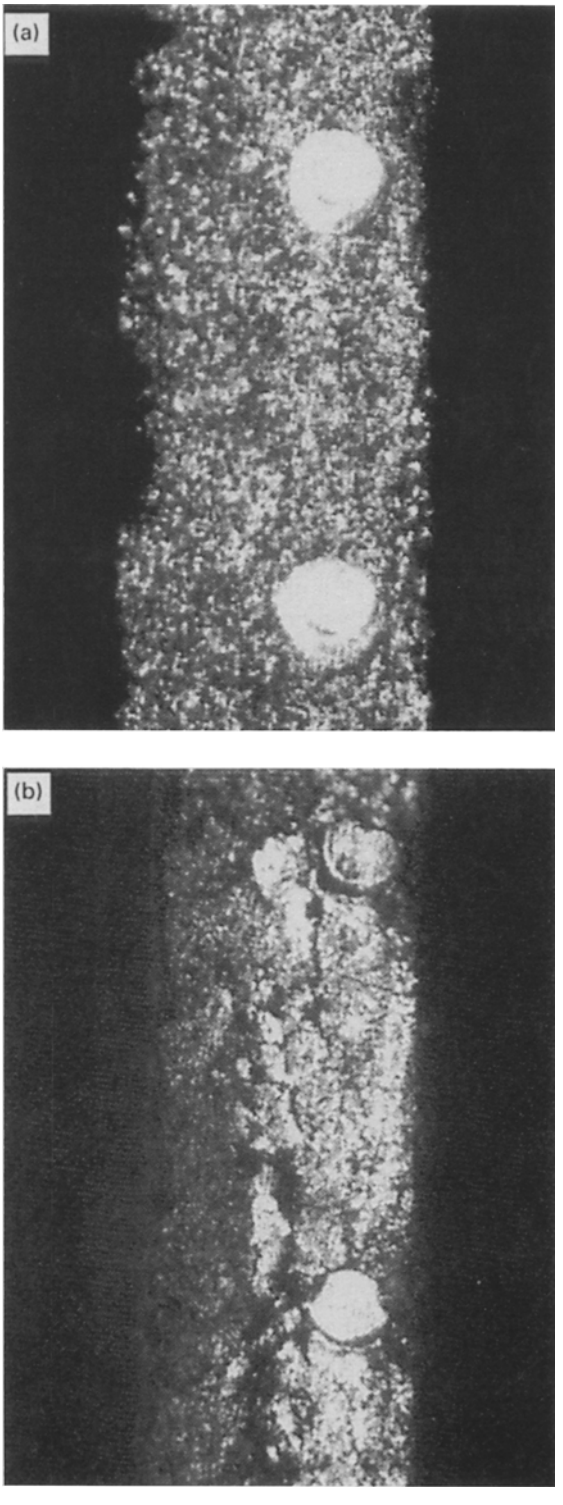

Fig. 7. Optical micrographs of (a) uncycled and (b) cycled nickel oxide electrode material. Electrode thickness is 0.94 mm.

The goal of the post-cycling experiments performed on electrode samples was to determine, through a series of modifications in the operating conditions, whether significant amounts of lost capacity could be recovered. All experiments were conducted in electrolytes of 5.9 M KOH plus 1.1 M LiOH. Modifying treatments applied serially included addition of surfactant to the electrolyte, washing of the electrode in KOH, and compression of the electrode.

Figure 8 compares the discharge behaviour of the electrode without any modifications (curve (a)) to experiments made under various modifying conditions (curves (b)–(e)). The effect of adding 1.1 g dm^{-3} Triton X-100 (curve (b)) is seen to be small, as is the effect of washing the electrode (curve (c)). The latter result is in contrast to the report of Dmitrenko *et al.* [13], who claimed that by washing in hot KOH, a recovery of capacity for cycled nickel oxide electrodes used in Zn/NiOOH cells could be obtained. It should be noted that their system used a KOH–LiOH electrolyte, and not the KOH–LiOH–K_2CO_3–KF system studied here. Details of the extent and method of capacity recovery were sparse as well. Note that the experiment for curve (c) was conducted under conditions of $C/15$ charge and $C/15$ discharge, in contrast to all other experiments reported here, which were conducted with $C/6$ charge and $C/6$ discharge.

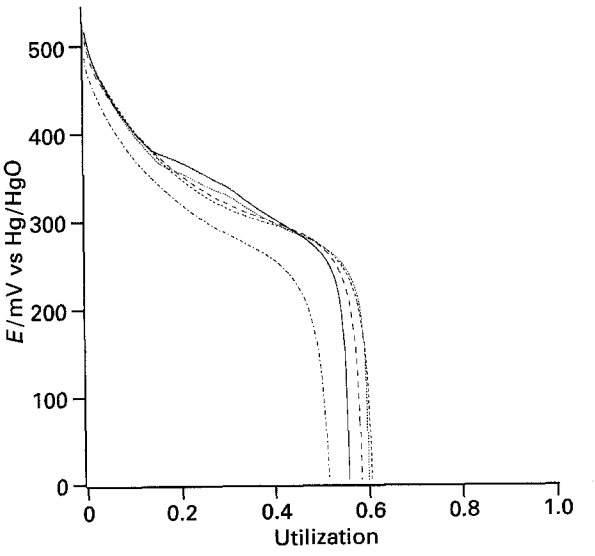

Fig. 8. Discharge curves showing the influence of various modifying conditions on electrode performance. Key: (——, (a)) no treatments, (·····, (b)) 1100 mg dm^{-3} Triton X-100, (– – –, (c)) after washing, (— — —, (d)) compression at 310 kPa and (– · – · –, (e)) compression at 2070 kPa.

Mechanical compression of the electrodes was also examined as a means to recover capacity. Figure 8 shows results for capacity tests under applied loads of $310\,kN\,m^{-2}$ (curve (d)) and $2070\,kN\,m^{-2}$ (curve (e)). The application of pressure does not appear to influence the discharge capacity a great deal, indicating that contact with isolated portions of the electrode cannot be easily reestablished in this way.

These experiments do not reveal the exact mechanism of mechanical degradation. Further investigations could help distinguish between various possibilities, such as (i) accelerated corrosion of the nickel sinter promoted by the presence of fluoride ions, (ii) insertion of zinc species between $Ni(OH)_2$ interplanar sheets and accompanying stress on the crystal structure, or (iii) enhanced rates of oxygen gas evolution associated with the $KOH–K_2CO_3–KF$ electrolyte, which could lead to accelerated sinter damage. Nickel oxide electrode pore blockage by ZnO and/or $Zn(OH)_2$ is of course a possible important cause of nickel oxide capacity loss in any type of electrolyte. It would be instructive to compare experiments in $KOH–K_2CO_3–KF$ electrolyte with those in pure KOH electrolyte, however Zn/NiOOH cells cycled with the usual concentration of KOH electrolyte are severely limited by zinc electrode problems and do not cycle for a sufficiently long time to reveal the degradation of the nickel oxide electrode observed in Zn/NiOOH cells with $KOH–K_2CO_3–KF$ electrolyte.

4. Summary and conclusions

In this work, nickel oxide electrodes that were cycled to failure in a Zn/NiOOH cell were characterized. This cell incorporated a novel electrolyte that significantly increased the cycle life of the zinc electrode [1]. An important question was the nature of the zinc species that was found to be deposited in the cycled nickel oxide electrodes. Photoelectron spectroscopy indicated that the form of zinc is ZnO and/or $Zn(OH)_2$. There have been reports in the literature that a nickel–zinc compound, 'nickel hydroxyzincate', may be responsible for the capacity degradation of nickel oxide electrodes in zinc/nickel oxide cells. Several methods were used to characterize this material, including photoelectron spectroscopy, Raman spectroscopy, and X-ray diffraction. The results obtained, while not fully definitive, suggest that the characterization of this material as a compound having nickel and zinc present in the same crystal lattice may not be correct. A better interpretation is that the material exists as a coprecipitate, or perhaps as an intercalation compound, with zinc species existing between the sheets of turbostratic nickel hydroxide. Evidence of a more convincing nature could be obtained through EXAFS measurements.

Considerable evidence was found for a strictly mechanical interpretation of the capacity degradation of the nickel oxide electrodes studied. The resistivity of cycled electrodes was substantially greater than that of uncycled ones. This increase is significant in that it implies that some active material may have lost electrical contact with the current collector, leading to a decrease in observed discharge capacity. Spatial variations of the resistivity increase were also recorded. Optical microscopy confirmed the presence of extensive mechanical degradation within some cycled electrode samples. Cell cycling experiments did not suggest that the capacity loss is due to a loss of wetting, however the experiments conducted with a surfactant were not exhaustive. Attempts to wash the electrode to remove precipitated zinc species, a strategy which has been reported to be effective in some Zn/NiOOH cell experiments, were found to have little effect. Compression of cycled nickel oxide electrodes, in an attempt to provide improved electrical contact between the active material and the current collector, was also found to yield little improvement. In summary, the capacity degradation of nickel oxide electrodes in Zn/NiOOH cells using novel, low-alkalinity electrolytes appears to be largely mechanical in nature, and possibly irreversible. The resistivity measurements indicate that the capacity loss varies spatially. If this interpretation of the failure of the nickel oxide electrode is correct, then the suggestions of Fritts [7, 8] and of Lanzi and Landau [9] may lead to improvement of the cycle life performance of the Zn/NiOOH cell; i.e., to use thinner electrodes and a stronger current collector structure. Such a strategy would probably lead to an increase in the weight of the cell per unit capacity, which is undesirable for applications requiring a high specific energy.

Acknowledgements

The authors thank D. Littlejohn of LBL for acquiring the Raman spectra. This work was supported by the Assistant Secretary for Energy Efficiency and Renewable Energy, Office of Transportation Technologies, Electric and Hybrid Propulsion Division of the U.S. Department of Energy under Contract No. DE-AC03-76SF00098.

References

[1] T. C. Adler, F. R. McLarnon and E. J. Cairns, *J. Electrochem. Soc.* **140** (1993) 289.
[2] E. Buder, *J. Appl. Electrochem.* **2** (1972) 301.
[3] I. Arulraj and D. C. Trivedi, *Int. J. Hydrogen Energy* **14** (1989) 893.
[4] B. E. Conway, M. A. Sattar and D. Gilroy, *Electrochim. Acta* **25** (1980) 973.
[5] G. Bronoel and J. Reby, *ibid.* **25** (1980) 973.
[6] K. Kinoshita, 'Electrochemical Oxygen Technology', John Wiley & Sons, New York (1992).
[7] D. H. Fritts, *J. Power Sources* **6** (1981) 327.
[8] *Idem, ibid.* **12** (1984) 267.
[9] O. Lanzi and U. Landau, *J. Electrochem. Soc.* **138** (1991) 2527.

[10] M. Natan, D. Belanger, M. Carpenter and M. Wrighton, *J. Phys. Chem.* **91** (1987) 1834.
[11] A. Briggs, *J. Appl. Electrochem.* **21** (1982) 999.
[12] V. Dmitrenko, M. Zubov, V. Barsukov and L. Sagoyan, *Elektrokhimiya* **23** (1987) 1240.
[13] V. Dmitrenko, M. Zubov, V. Baulov, L. Sagoyan and V. Barsukov, *ibid.* **19** (1983) 852.
[14] H. Bode, K. Dehmelt and J. Witte, *Electrochim. Acta* **11** (1966) 1079.
[15] V. Romanov, *Zh. Priklad. Khim.* **34** (1961) 1317.
[16] V. Kozyrin, A. Bachaev, S. Bazarov and V. Flerov, *Elektrokhimiya* **25** (1989) 267.
[17] V. Gud, V. Nikol'skii, Z. Arkhangel'skaya and G. Reshetova, *Zh. Priklad. Khim.* **63** (1990) 2650.
[18] C. Faure, C. Delmas and M. J. Fouassier, *J. Power Sources* **35** (1991) 279.
[19] T. Adler, unpublished data, Lawrence Berkeley Laboratory, Berkeley, CA, March (1994).
[20] C. Johnston and P. R. Graves, *Appl. Spectroscopy* **44** (1990) 105.
[21] A. H. L. Goff, S. Joiret, B. Saidani and R. Wiart, *J. Electroanal. Chem.* **263** (1989) 127.
[22] K. S. Kim and N. Winograd, *Surf. Sci.* **43** (1974) 625.
[23] T. Dickenson, A. F. Povey and P. M. A. Sherwood, *J. Chem. Soc. Faraday Trans. I* **73** (1977) 327.
[24] T. L. Barr, *J. Phys. Chem.* **82** (1978) 1801.
[25] K. S. Kim, W. E. Baitinger, J. W. Amy and N. Winograd, *J. Electron Spect. Rel. Phenom.* **5** (1974) 351.
[26] B. P. Lochel and H. H. Strehblow, *J. Electrochem. Soc.* **131** (1984) 713.
[27] N. S. McIntyre, T. E. Rummery, M. G. Cook and D. Owen, *J. Electrochem. Soc.* **123** (1976) 1164.
[28] D. Briggs and M. P. Seah (eds.), 'Practical Surface Analysis, Volume 1: Auger and X-ray Photoelectron Spectroscopy', John Wiley & Sons, Chichester (1990).
[29] C. D. Wagner, W. M. Riggs, L. E. Davis, J. F. Moulder and G. E. Muilenberg, 'Handbook of X-ray Photoelectron Spectroscopy', Physical Electronics Division, Perkin–Elmer Coporation, Eden Prairie, Minnesota (1979).
[30] J. H. Linn and W. E. Swartz Jr., *Applic. Surf. Sci.* **20** (1984) 154.